NANO LETTERS

Letter

pubs.acs.org/NanoLett

# Symmetric and Asymmetric Au–AgCdSe Hybrid Nanorods

Shan Liang,[†] Xiao-Li Liu,[†] Yue-Zhou Yang,[†] Ya-Lan Wang,[†] Jia-Hong Wang,[†] Zhong-Jian Yang,[†] Liang-Bing Wang,[‡] Shuang-Feng Jia,[§] Xue-Feng Yu,[†,*] Li Zhou,[†] Jian-Bo Wang,[†,§] Jie Zeng,[‡,∥,*] Qu-Quan Wang,[†,*] and Zhenyu Zhang[‡,⊥]

[†]Department of Physics and Key Laboratory of Artificial Micro- and Nano-Structures of Ministry of Education, Wuhan University, Wuhan 430072, Hubei, People's Republic of China

[‡]Hefei National Laboratory for Physical Sciences at the Microscale, University of Science and Technology of China, Hefei 230026, Anhui, People's Republic of China

[§]Center for Electron Microscopy, Wuhan University, Wuhan 430072, Hubei, People's Republic of China

[∥]Department of Chemical Physics, University of Science and Technology of China, Hefei 230026, Anhui, People's Republic of China

[⊥]School of Applied Sciences and Engineering, Harvard University, Cambridge, Massachusetts 02138, United States

Supporting Information

**ABSTRACT:** This paper describes a facile method for synthesis of Au–AgCdSe hybrid nanorods with controlled morphologies and spatial distributions. The synthesis involved deposition of Ag tips at the ends of Au nanorod seeds, followed by selenization of the Ag tips and overgrowth of CdSe on these sites. By simply manipulating the pH value of the system, the AgCdSe could selectively grow at one end, at both the ends or on the side surface of a Au nanorod, generating a mike-like, dumbbell-like, or toothbrush-like hybrid nanorod, respectively. These three types of Au–AgCdSe hybrid nanorods displayed distinct localized surface plasmon resonance and photoluminescence properties, demonstrating an effective pathway for maneuvering the optical properties of nanocrystals.

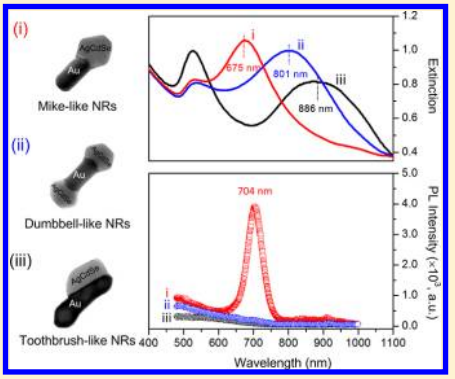


**KEYWORDS:** *Hybrid, nanocrystals, metal–semiconductor, surface plasmon resonance, photoluminescence*

Hybrid nanostructures that integrate two or more nanoscale components have recently attracted much attention owing to the synergistic properties induced by interactions between these objects. Promising examples of such structures are metal–semiconductor hybrid nanocrystals, in which a metal and its semiconductor counterpart are closely coupled in an effort to produce intriguing behaviors and functionalities far beyond those of their individual counterparts.[1−12] For example, metal tips on semiconductor nanorods can serve as anchor points for electrical connections or for head-to-end self-assembly into complex structures,[3,13] while improved charge separation at the metal–semiconductor interface can enhance its photocatalytic activities[14] or modify its nonlinear optical response.[15] Furthermore, addition of semiconductor tips to metal nanocrystals can greatly improve the stability of metal nanocrystals against aging at a high temperature[16] and maneuver the fascinating optical properties of metal nanocrystals known as surface plasmon resonance (SPR).[16,17] As many of their physical and chemical properties are highly dependent on the size, shape, composition, and spatial distribution of each component, the synthetic strategy of such metal–semiconductor hybrid nanonanocrystals has become increasingly important. Thanks to the efforts from a large number of research groups, a myriad of methods have been developed, including those based on selective anisotropic growth,[3,4,15−23] formation of micelles,[24] oxidation-directed decomposition,[25] phase segregation induced by ripening,[26,27] photochemical fabrication,[28] diffusion process,[29] phase-transfer protocol,[30] in situ sulfuration,[16] and cation-exchange technology.[17,31] Although all these methods are capable of generating high-quality hybrid nanocrystals, it still remains a grand challenge to spatially control the component distribution and thus regulate the symmetry of the hybrid nanocrystals, especially for systems constructed using the same materials.

With Au nanorods as the starting seeds, here we describe a facile approach to the synthesis of Au–AgCdSe hybrid nanorods with the semiconductor portion (i.e., AgCdSe) growing either at one end, at both the ends, or on the side surface of a Au nanorod. We chose Au nanorods as our initial material because they have received great interests in a wide variety of fields due to their tunable surface plasmon resonance (SPR) that is sensitive to both the aspect ratio of the nanorods and the coating materials.[32] The synthesis involved deposition

**Received:** July 10, 2012
**Revised:** August 30, 2012
**Published:** September 4, 2012

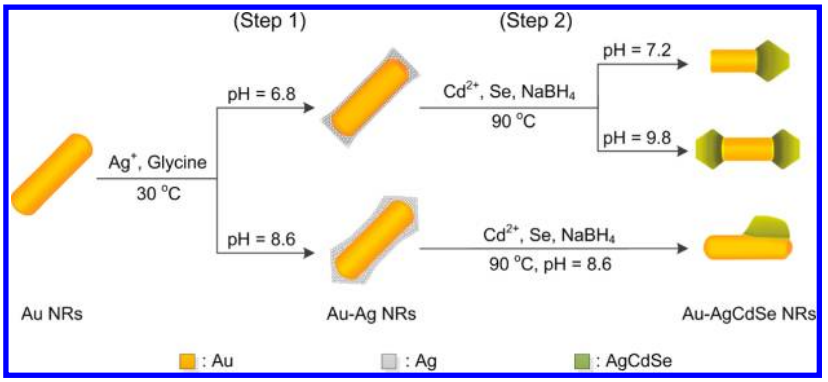


**Figure 1.** Schematic illustration of the syntheses of three different types of Au−AgCdSe hybrid nanorods.

of Ag tips at the ends of a Au nanorod, followed by selenization of the Ag tips and overgrowth of CdSe on these sites (see Supporting Information for experimental details). By simply manipulating the pH value of the system, we found that the reaction kinetics could be well controlled. As such, Au−AgCdSe hybrid nanorods with three distinct structures could be produced under otherwise similar conditions: mike-like nanorods with AgCdSe growing at only one end of a Au nanorod; dumbbell-like nanorods with AgCdSe growing at both the ends of a Au nanorod; and toothbrush-like nanorods with AgCdSe growing on the side surface, near one end of a Au nanorod. These Au−AgCdSe hybrid nanorods displayed substantially different SPR and photoluminescence (PL) properties. This synthesis provides a convenient and environmentally benign route to large-scale production because it does not involve inert atmospheric gases, organic solvents, or phase-transfer processes.

Figure 1 schematically illustrates the reaction pathways that lead to the formation of three different types of Au−AgCdSe hybrid nanorods. The synthesis is based on a two-step seed-mediated growth. In the first step, Au−Ag bimetallic nanorods were prepared by consecutively adding $AgNO_3$, glycine, and NaOH to an aqueous dispersion of Au nanorods containing hexadecyltrimethylammonium bromide (CTAB) at 30 °C. As shown in Figure 2a, the starting Au nanorods were 15 ± 2 nm in width and 58 ± 6 nm in length. They were relatively uniform in terms of size and aspect ratio with a variation less than 13%. Right after the addition of NaOH (for the synthesis of mike-like Au−AgCdSe nanorods, the pH was manipulated to 6.8), the solution turned from dark red to firebrick within 10 min. After further reaction for 10 h, we obtained Au−Ag bimetallic nanocrystals with more-or-less an "I" shape and an average length of 60 ± 7 nm (Figure 2b). The Ag tended to deposit at both the ends of a Au nanorod although it covered throughtout the surface of the nanorod seed. The insets in Figure 2a,b show the tip morphologies of Au and Au−Ag nanorods, respectively.

The second step involved a selenization reaction of the Ag tips of the as-prepared I-shaped nanorods associated with a selective growth of CdSe bumps at only one end of the nanorods. In a typical synthesis, we mixed an aqueous solution of the as-prepared I-shaped Au−Ag nanorods with specific amounts of selenium powder, $Cd(NO_3)_2$, and $NaBH_4$. The reaction was allowed to proceed at 90 °C for 2 h under ambient conditions and can be described by the following equations

$$2Ag + Se \rightarrow Ag_2Se \quad (1)$$

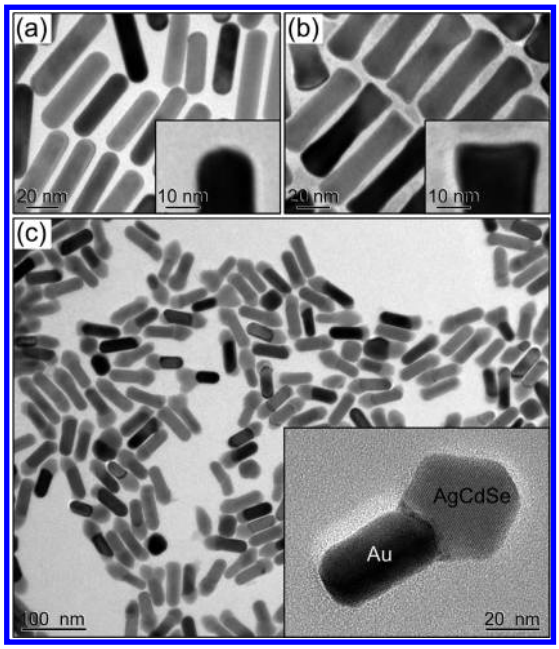


**Figure 2.** TEM images of (a) the Au nanorods (15 nm × 58 nm in width and length, respectively), (b) the I-shaped Au−Ag nanorods (with a mean length of 60 nm), and (c) the mike-like Au−AgCdSe nanorods (with a mean size of 24 nm for the AgCdSe bumps and a mean length of 41 nm for the Au rods).

$$4Cd^{2+} + 4Se + BH_4^- + 3H_2O \rightarrow 4CdSe + B(OH)_3 + 7H^+ \quad (2)$$

On the basis of the change in Gibbs free energy ($\Delta G^\circ$ = −49.4 kJ/mol at 298 K),[33] $Ag_2Se$ is expected to form spontaneously when Au−Ag nanorods and Se powder encounter in the solution. Once formed, $Ag_2Se$ then acted as the seeds for overgrowth of CdSe in the presence of $BH_4^-$ as a reducing agent (eq 2). Interestingly, it was found that CdSe selectively grew only at one end of each nanorod to form an asymmetric structure with a mike-like shape (Figure 2c) rather than at both the ends to form a symmetric, I-shaped nanorod when the pH was set at 7.2. The average size of the CdSe bumps is ∼24 nm. Note that the other end at which no CdSe deposited also lost its original "I" shape (see inset of Figure 2c), indicating that a shape transformation process must have taken place in this step.

To elucidate the formation mechanism of mike-like nanorods shown in Figure 2c, we monitored the evolution of shape by


dx.doi.org/10.1021/nl3025505 | Nano Lett. 2012, 12, 5281−5286

drawing samples from the solution at different stages of the reaction, followed by extinction test and transmission electron microscopy (TEM) imaging. Figure 3a shows the extinction

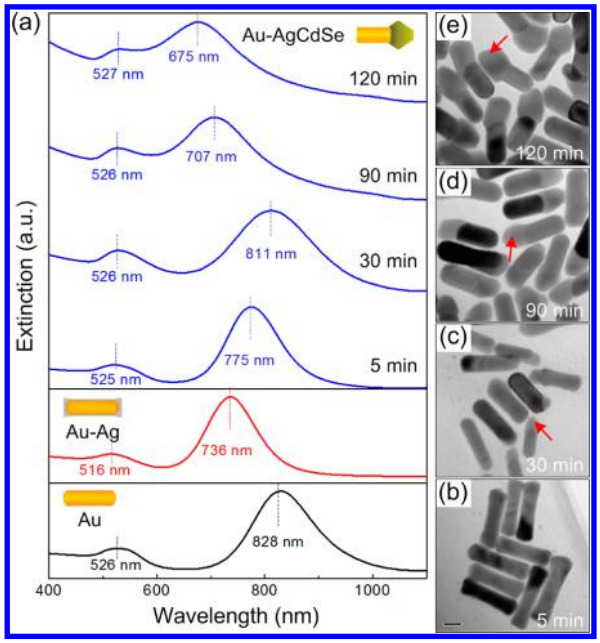


**Figure 3.** (a) UV–vis extinction spectra taken from the Au nanorods, the I-shaped Au–Ag nanorods, and the products obtained at different reaction points for synthesis of mike-like Au–AgCdSe nanorods. (b–e) TEM images of the corresponding products. The scale bar is 20 nm in (b) and applies to all TEM images. The red arrows indicate the positions of AgCdSe components.

spectra of products obtained at different reaction points. The longitudinal surface plasmon resonance (LSPR) band of the original Au nanorods appeared at ~828 nm, and the transverse surface plasmon resonance (TSPR) band was centered at ~526 nm. With the deposition of silver, both the LSPR and TSPR bands blue shifted.[17,34] Once the second step was initiated, the LSPR band first red shifted to ~811 nm at 30 min and then blue shifted to ~675 nm at 120 min. TEM images of the corresponding products are shown in Figure 3b–e. Earlier in the reaction (at 5 min), nanorods with two enlarged ends were observed (Figure 3b). Energy dispersive X-ray (EDX) analyses on a single nanorod indicated that Se was only distributed at the ends of the nanorod (Supporting Information Figure S1). No signal for Se was detected in the central region. All the data support the formation of Au–$Ag_2Se$ hybrid nanorods. It is believed that the formation of $Ag_2Se$ tips should be responsible for the red shift of the LSPR band in the early stage as $Ag_2Se$ has a relatively high dielectric constant.[35,36] As the reaction progressed, one of the ends gradually grew larger while the other shrank (at 30 min, Figure 3c) and completely disappeared (at 90 min, Figure 3d). Ultimately, mike-like hybrid nanorods formed at 120 min (Figure 3e) where the semiconductor component (i.e., the fat bump) was lighter in contrast than the Au component due to their difference in electron density. Note that the width of the Au nanorods increased while the length decreased during the synthesis, which eventually caused the blue shift of the LSPR band at the later stage.

We further used a number of tools involving high-angle annular dark-field scanning TEM (HAADF-STEM), EDX, X-ray diffraction (XRD), and high-resolution TEM (HRTEM) to analyze the chemical compositions and characterize the structures of the mike-like hybrid nanorod. The distributions of Au, Ag, Cd, and Se were clearly resolved by EDX elemental mapping (Figure 4a–d), line-scan EDX spectra (Figure 4e),

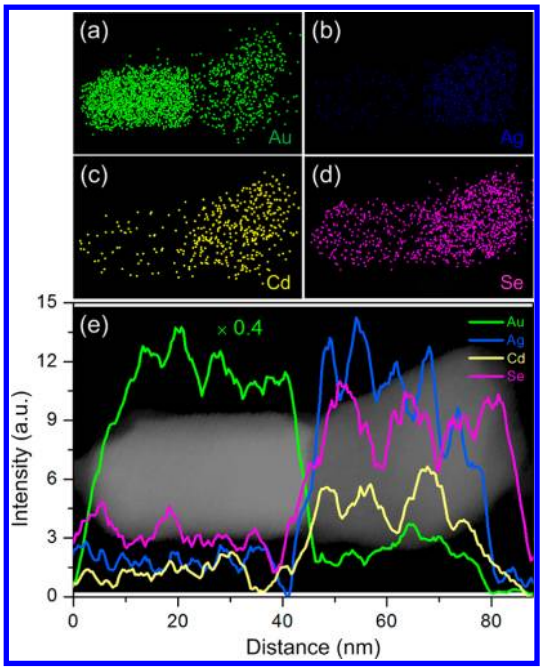


**Figure 4.** (a–d) EDX elemental maps of Au, Ag, Cd, and Se in an individual mike-like Au–AgCdSe nanorod. (e) HAADF-STEM image of this nanorod with line profiles of Au, Ag, Cd, and Se.

and the corresponding HAADF-STEM image (Figure 4e). All the data suggests that the rod portion was made of Au while the bump was composed of Ag, Cd, and Se. Since Ag, Cd, and Se were evenly distributed throughout the bump, we believe that they have formed an alloy phase. The average composition of the bumps determined by EDX analysis of 12 nanocrystals was $Ag_{0.8}Cd_{0.6}Se$. XRD pattern of the Au–AgCdSe hybrid nanorods indicates that the Au components are in a face-centered cubic (fcc) form while the AgCdSe components are hexagonal (Supporting Information Figure S2). Supporting Information Figure S3 shows HRTEM images of a mike-like Au–AgCdSe nanorod. The fringe spacing of 2.0 Å can be indexed to the {200} reflection of fcc Au, while the spacing of 2.2 and 2.6 Å may correspond to the {110} and {102} reflections of hexagonal AgCdSe.

The alloy of AgCdSe could be formed through two different mechanisms: cation exchange of $Cd^{2+}$ ions with $Ag_2Se$ and ripening of $Ag_2Se$ at the ends of a nanorod. The exchange between two cations involving $Cd^{2+}$ and $Ag^+$, $Cd^{2+}$ and $Cu^{2+}$, and $Cd^{2+}$ and $Pb^{2+}$ has been demonstrated to be a general and reversible phenomenon in semiconductor nanocrystals, which can be driven by quite a few experimental factors such as the concentration of cations, the solvent, and the surfactant.[37] In this study, as described above, $Ag_2Se$ tips formed at both ends of each Au nanorod prior to the formation of CdSe. Considering the large difference in concentration between free $Ag^+$ and $Cd^{2+}$ ions in the solution, we believe that the $Ag^+$ ions in the $Ag_2Se$ tips would be partially replaced by $Cd^{2+}$ in the following reaction to form AgCdSe alloy. In addition, since the products changed from I-shaped nanorods to mike-like ones during the synthesis, the shape transformation must have


dx.doi.org/10.1021/nl3025505 | Nano Lett. 2012, 12, 5281–5286

involved an etching process. Potentially, at one end of the nanorod $Ag_2Se$ is oxidized by a Se atom located at the other end of the rod. In this process, the conductive metal rod offers an effective pathway for electron transfer. The Se stom is consequently reduced to $Se^{2-}$ while the $Ag_2Se$ releases two $Ag^+$ ions and a Se atom to solution. At the same time, the released $Ag^+$ ions would mix into the solution and coprecipitate with both $Cd^{2+}$ and $Se^{2-}$ ions at the opposite end to form AgCdSe alloy. This process, which can be considered as ripening of $Ag_2Se$ tips governed by an electrochemical driving force, would eventually lead to the formation of asymmetric, mike-like Au–AgCdSe nanorods shown in Figure 2c. We further used Au nanorods with either a shorter (45 ± 6 nm) or a longer (66 ± 7 nm) length as the seeds to demonstrate the generality of this method for the preparation of asymmetric Au–AgCdSe hybrid nanocrystals. The results were shown in Supporting Information Figures S4 and S5. As expected, mike-like Au–AgCdSe nanorods were obtained, regardless of the length of the nanorod seeds. Similarly, when using spherical Au nanocrystals as the seeds, we obtained Janus-like Au–AgCdSe hybrid nanocrystals (Supporting Information Figure S6).

Note that $H^+$ ions were produced during the overgrowth of CdSe in the second step (eq 2), which gives us the ability to control the reducing power of $BH_4^-$ and thus manipulate the reaction kinetics by simply adjusting the pH value of the solution. When the pH was increased, the reducing power of $BH_4^-$ and the subsequent formation rate of CdSe were boost up. As such, it is not unreasonable to assume that once the formation rate of CdSe had overwhelmingly exceeded the ripening rate of $Ag_2Se$, CdSe could deposit directly on all of the $Ag_2Se$ tips. Our experiment conducted at a higher pH (9.8 instead of 7.2 at which the mike-like nanorods formed) confirmed this argument. As shown in Figure 5a, the higher pH

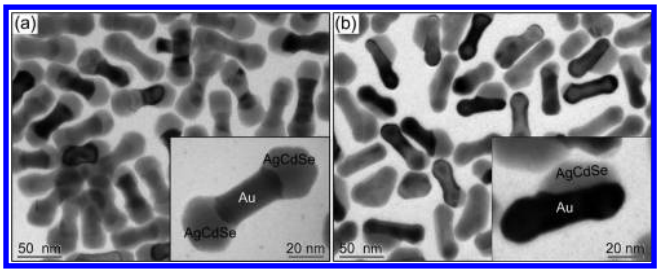


**Figure 5.** TEM images of (a) dumbbell-like and (b) toothbrush-like Au–AgCdSe nanorods.

produced dumbbell-like, hybrid nanorods with semiconductor portions (most likely composed of AgCdSe alloy as well) grown at both the ends of a Au nanorod. In addition, the reaction kinetics of the first step (for growing Ag) also relies on the pH as the reducing power of glycine is sensitive to the pH value.[38] Since a higher pH value makes glycine a stronger reductant, the reduction of Ag could be boosted up under this condition. When the experiment was conducted at pH = 8.6 (instead of 6.8 at which the I-shaped Au–Ag nanorods formed), because of the faster reduction of Ag a larger number of Ag atoms would be generated at any moment to interact with the surface of Au nanorods, thus promoting the collision of Ag atoms with a larger portion of the side surface of Au nanorods to form more active growth sites there. As such, differing from the I-shaped Au–Ag nanorods, the shuttle-shaped ones with a higher coverage density of Ag on the side surface were preferentially produced (Supporting Information Figure S7).[39] Further growth of CdSe led to the formation of toothbrush-like, hybrid nanorods with the semiconductor portion grown on the side surface, near one end of a Au nanorod (Figure 5b). It is not hard to understand this result by considering the fact that the selenization reaction should be preferentially initiated on the side surface rather than at the ends of a nanorod due to the difference in surface areas and thus different collision frequencies with the Se atoms. EDX analyses reveal that the average compositions of the AgCdSe components of the dumbbell-like and toothbrush-like nanorods were the same as that of mike-like nanorods (12 nanocrystals were examed for each case, data not shown). It is worth pointing out that all three kinds of hybrid nanocrystals (those shown in Figures 1c and 5a,b) have high yields (>85% for each case), demonstrating the feasibility of our approach for the synthesis of Au–AgCdSe hybrid nanorods with controlled structures and symmetries.

The hybrid morphology associated with the new Au–AgCdSe nanorods makes them interesting candidates for investigating the shape dependence of extinction and PL properties. Figure 6a gives UV–vis spectra taken from aqueous suspensions of Au–AgCdSe hybrid nanorods at roughly the same particle concentration but in three distinct shapes. While the positions of their TSPR bands were located at the same wavelength, the mike-like nanorods showed a LSPR band at a relatively shorter wavelength relative to those of dumbbell-like nanorods and toothbrush-like nanorods. The toothbrush-like nanorods exhibited a stronger TSPR peak and a weaker LSPR peak as compared to the other two cases, possibly because in the case of a toothbrush-like nanorod, the two ends where the TSPR mode is located were clear while the side surface where the LSPR band is located was blocked by a AgCdSe bump.

Figure 6b compares the PL spectra of the three different nanocrystals. Interestingly, only the mike-like nanorods showed an excitonic band emission peaked at ~704 nm with a full width at half-maximum of ~45 nm, which slightly blue-shifted from that of bulk CdSe (1.74 eV).[40,41] In contrast, no PL peaks were observed for dumbbell-like nanorods or toothbrush-like nanorods. It has been demonstrated that the strong interaction between exciton and plasmon states in a metal–semiconductor hybrid nanostructure can result in either enhancement or quenching in PL.[3,4] The PL quenching can be attributed to the energy transfer from exciton (in the semiconductor portion) to plasmon (in the metal portion) via resonance coupling, as opposed to the PL enhancement arisen from coupled field stimulation with the metal portion. In this study, the quenching effect is believed to work for all the three kinds of hybrid nanorods because they have the similar short distance between AgCdSe and Au portions. But for the case of mike-like nanorods, the LSPR peak (~675 nm) is very near the band edge of CdSe exciton absorption (~710 nm).[40,41] As such, the observed exciton emission is probably due to the coupled field enhancement from the Au portion of the nanorods. To verify this hypothesis, we also tested the PL properties of mike-like Au–AgCdSe nanorods with both shorter (see the top row of Supporting Information Figure S4) and longer (see the top row of Supporting Information Figure S5) lengthes. The results were shown in Supporting Information Figure S8. As expected, no obvious PL peak was detected for the shorter nanorods due to the deviation of their LSPR band (635 nm) from the PL peak (710 nm). For the longer nanorods, a relatively weak PL peak appeared at 710 nm, possibly because the extinction intensity of these nanorods was still high at 710 nm although


dx.doi.org/10.1021/nl3025505 | *Nano Lett.* 2012, 12, 5281–5286

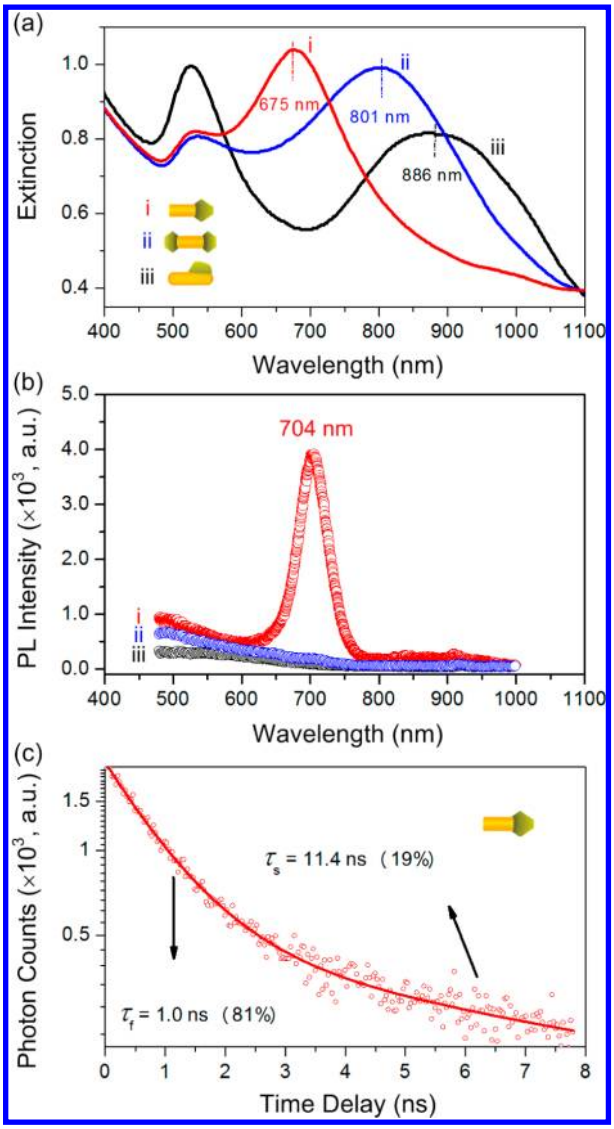


**Figure 6.** (a) UV–vis extinction spectra of mike-like (curve i), dumbbell-like (curve ii), and toothbrush-like (curve iii) Au–AgCdSe nanorods. (b) PL spectra of mike-like (curve i), dumbbell-like (curve ii), and toothbrush-like (curve iii) Au–AgCdSe nanorods. (c) Time-resolved PL spectrum of the mike-like Au–AgCdSe nanorods.

their LSPR band had red shifted to 748 nm (Supporting Information Figure S5a). A time-resolved fluorescence experiment was performed to further investigate the effect of exciton-plasmon interaction (Figure 6c). Two decay processes with lifetimes of 1.0 ns (81% emission) and 11.4 ns (19% emission) were observed for the mike-like nanorods, which are much faster than those of free semiconductor quantum dots.[42] Such great decrease in the excitonic emission lifetime further demonstrates the strong interaction between the Au and AgCdSe portions.[43]

In summary, we have demonstrated a simple and versatile method for generating Au–AgCdSe hybrid nanorods with well-controlled morphologies and symmetries. By simply manipulating the pH value at which the Ag and CdSe were deposited on the Au nanorod seeds, we could achieve selective growth of AgCdSe at one end, at both the ends, or on the side surface of a Au nanorod. As such, we obtained Au–AgCdSe hybrid nanorods with three distinctive structures under otherwise similar experimental conditions: mike-like, dumbbell-like, and toothbrush-like nanorods, respectively. These hybrid nanorods are attractive for applications in photonics as they displayed different LSPR peaks compared to Au nanorods and distinct PL properties. We believe that this approach based on kinetically controlled, seed-mediated growth and selenization can be extended to other metal–semiconductor systems to generate hybrid nanocrystals with rationally designed morphologies and, thus, enhanced photocatalytic and photovoltaic capabilities.

## ■ ASSOCIATED CONTENT

### Supporting Information

Additional information and figures. This material is available free of charge via the Internet at http://pubs.acs.org.

## ■ AUTHOR INFORMATION

### Corresponding Author

*E-mail: (J.Z.) zengj@ustc.edu.cn; (X.-F.Y.) yxf@whu.edu.cn; (Q.-Q.W.) qqwang@whu.edu.cn.

### Notes

The authors declare no competing financial interest.

## ■ ACKNOWLEDGMENTS

This work was supported by the NSFC (11034006, 10904119, 21121003, 21203173, and 61008043), the National Program on Key Science Research of China (2011CB922201 and 2011CB921403), and the Key Project of the Ministry of Education of China (708063).

## ■ REFERENCES

(1) Lee, J.; Hernandez, P.; Lee, J.; Govorov, A. O.; Kotov, N. A. *Nat. Mater.* **2007**, *6*, 291–295.
(2) Zhang, J.; Tang, Y.; Lee, K.; Ouyang, M. *Nature* **2010**, *466*, 91–95.
(3) Mokari, T.; Rothenberg, E.; Popov, I.; Costi, R.; Banin, U. *Science* **2004**, *304*, 1787–1790.
(4) Mokari, T.; Sztrum, C. G.; Salant, A.; Rabani, E.; Banin, U. *Nat. Mater.* **2005**, *4*, 855–863.
(5) Shaviv, E.; Banin, U. *ACS Nano* **2010**, *4*, 1529–1538.
(6) Jin, Y.; Gao, X. *Nat. Nanotechnol.* **2009**, *4*, 571–576.
(7) Lee, J.-S.; Shevchenko, E. V.; Talapin, D. V. *J. Am. Chem. Soc.* **2008**, *130*, 9673–9675.
(8) Khon, E.; Mereshchenko, A.; Tarnovsky, A. N.; Acharya, K.; Klinkova, A.; Hewa-Kasakarage, N. N.; Nemitz, I.; Zamkov, M. *Nano Lett.* **2011**, *11*, 1792–1799.
(9) Shaviv, E.; Schubert, O.; Alves-Santos, M.; Goldoni, G.; Di Felice, R.; Vallée, F.; Del Fatti, N.; Banin, U.; Sönnichsen, C. *ACS Nano* **2011**, *5*, 4712–4719.
(10) Wang, H.; Sun, Z.; Lu, Q.; Zeng, F.; Su, D. *Small* **2012**, *8*, 1167–1172.
(11) Wang, D.; Li, Y. *J. Am. Chem. Soc.* **2010**, *132*, 6280–6281.
(12) Choi, S. H.; Kim, E. G.; Hyeon, T. *J. Am. Chem. Soc.* **2006**, *128*, 2520–2521.
(13) Figuerola, A.; Franchini, I. R.; Fiore, A.; Mastria, R.; Falqui, A.; Bertoni, G.; Bals, S.; Van Tendeloo, G.; Kudera, S.; Cingolani, R.; Manna, L. *Adv. Mater.* **2009**, *21*, 550–554.
(14) Costi, R.; Saunders, A. E.; Elmalem, E.; Salant, A.; Banin, U. *Nano Lett.* **2008**, *8*, 637–641.
(15) Yang, J.; Elim, H. I.; Zhang, Q.; Lee, J. Y.; Ji, W. *J. Am. Chem. Soc.* **2006**, *128*, 11921–11926.
(16) Zeng, J.; Tao, J.; Su, D.; Zhu, Y.; Qin, D.; Xia, Y. *Nano Lett.* **2011**, *11*, 3010–3015.
(17) Li, M.; Yu, X.-F.; Liang, S.; Peng, X.-N.; Yang, Z.-J.; Wang, Y.-L.; Wang, Q.-Q. *Adv. Funct. Mater.* **2011**, *21*, 1788–1794.
(18) Habas, S. E.; Yang, P.; Mokari, T. *J. Am. Chem. Soc.* **2008**, *130*, 3294–3295.

(19) Fan, F.-R.; Ding, Y.; Liu, D.-Y.; Tian, Z.-Q.; Wang, Z. L. *J. Am. Chem. Soc.* **2009**, *131*, 12036−12037.
(20) Kuo, C.-H.; Hua, T.-E.; Huang, M. H. *J. Am. Chem. Soc.* **2009**, *131*, 17871−17878.
(21) Sun, Z.; Yang, Z.; Zhou, J.; Yeung, M. H.; Ni, W.; Wu, H.; Wang, J. *Angew. Chem., Int. Ed.* **2009**, *48*, 2881−2885.
(22) Zeng, J.; Huang, J.; Liu, C.; Wu, C. H.; Lin, Y.; Wang, X.; Zhang, S.; Hou, J.; Xia, Y. *Adv. Mater.* **2010**, *22*, 1936−1940.
(23) AbouZeid, K. M.; Mohamed, M. B.; El-Shall, M. S. *Small* **2011**, *7*, 3299−3307.
(24) Gu, H.; Yang, Z.; Gao, J.; Chang, C. K.; Xu, B. *J. Am. Chem. Soc.* **2005**, *127*, 34−35.
(25) Yu, H.; Chen, M.; Rice, P. M.; Wang, S. X.; White, R. L.; Sun, S. *Nano Lett.* **2005**, *5*, 379−382.
(26) Gu, H.; Zheng, R.; Zhang, X.; Xu, B. *J. Am. Chem. Soc.* **2004**, *126*, 5664−5665.
(27) Peng, S.; Lei, C.; Ren, Y.; Cook, R. E.; Sun, Y. *Angew. Chem., Int. Ed.* **2011**, *50*, 3158−3163.
(28) Pacholski, C.; Kornowski, A.; Weller, H. *Angew. Chem., Int. Ed.* **2004**, *43*, 4774−4777.
(29) Yang, J.; Ying, J. Y. *J. Am. Chem. Soc.* **2010**, *132*, 2114−2115.
(30) Yang, J.; Sargent, E. H.; Kelley, S. O.; Ying, J. Y. *Nat. Mater.* **2009**, *8*, 683−689.
(31) Zhang, J.; Tang, Y.; Lee, K.; Ouyang, M. *Science* **2010**, *327*, 1634−1638.
(32) Jana, N. R.; Gearheart, L.; Murphy, C. J. *J. Phys. Chem. B* **2001**, *105*, 4065−4067.
(33) Neshkova, M. T.; Nikolova, V. D.; Bond, A. M.; Petrov, V. *Electrochim. Acta* **2005**, *50*, 5606−5615.
(34) Huang, Y.-F.; Lin, Y.-W.; Chang, H.-T. *Nanotechnology* **2006**, *17*, 4885−4894.
(35) Burda, C.; Chen, X.; Narayanan, R.; El-Sayed, M. A. *Chem. Rev.* **2005**, *105*, 1025−1102.
(36) Pastoriza-Santos, I.; Liz-Marzán, L. M. *Nano Lett.* **2002**, *2*, 903−905.
(37) Son, D. H.; Hughes, S. M.; Yin, Y.; Paul Alivisatos, A. *Science* **2004**, *306*, 1009−1012.
(38) Huang, Y. F.; Huang, K. M.; Chang, H. T. *J. Colloid Interface Sci.* **2006**, *301*, 145−154.
(39) Li, M.; Zhang, Z. S.; Zhang, X.; Li, K. Y.; Yu, X. F. *Opt. Express* **2008**, *16*, 14288−14293.
(40) Chen, R.; Bakti Utama, M. I.; Peng, Z.; Peng, B.; Xiong, Q.; Sun, H. *Adv. Mater.* **2011**, *23*, 1404−1408.
(41) Pan, A.; Liu, R.; Zhang, Q.; Wan, Q.; He, P.; Zacharias, M.; Zou, B. *J. Phys. Chem. C* **2007**, *111*, 14253−14256.
(42) Gong, H. M.; Zhou, Z. K.; Song, H.; Hao, Z. H.; Han, J. B.; Zhai, Y. Y.; Xiao, S.; Wang, Q. Q. *J. Fluoresc.* **2007**, *17*, 715−720.
(43) Fedutik, Y.; Temnov, V.; Schöps, O.; Woggon, U.; Artemyev, M. *Phys. Rev. Lett.* **2007**, *99*, 136802.